Chapter 13
Green Synthesis of Nanoparticles and Their Application for Sustainable Environment

Ardhendu Sekhar Giri and Sankar Chakma

Contents

A. S. Giri · S. Chakma (✉)
Department of Chemical Engineering, Indian Institute of Science Education and Research, Bhopal, M.P., India
e-mail: schakma@iiserb.ac.in

Inamuddin, A. M. Asiri (eds.), *Nanotechnology-Based Industrial Applications of Ionic Liquids*, Nanotechnology in the Life Sciences,
https://doi.org/10.1007/978-3-030-44995-7_13

13.1 Introduction

The nanomaterials have unique physicochemical, optical, and magnetic properties that are governed by the shape, size, and distribution of the nanoparticles (NPs). Due to these unique properties, nanotechnology has been used as one of the advanced and popular research areas (Daniel et al. 2004; Kumar et al. 2003). NPs have significantly a large surface area-to-volume ratio due to small size, and it considerably changes their properties (e.g., mechanical properties, catalytic activity, biological, electrical, and thermal conductivity) as compared to their bulk form (Perez et al. 2005). NPs are also used as catalysts for chemical reactions, sensors, pharmaceutical products, imaging for medical diagnostic, and medical treatment protocols. Some of the popular metallic nanoparticles such as gold (Au), silver (Ag), platinum (Pt), and palladium (Pd) are being comprehensively used in making the different electronic devices, pharmaceuticals, and grease paints. Gold NPs (AuNPs) have also been used in manufacturing pharmaceuticals but also in biomedical applications (Sperling et al. 2008; Puvanakrishnan et al. 2012). Silver nanoparticles (AgNPs) are being used to promote the faster spiral healing as they have anti-inflammatory and antibacterial properties for which the AgNPs are integrated into commercialized wound dressing kits, preparation of pharmaceutical, and medical transplant coverings (Pollini et al. 2008; Asha Rani et al. 2009). Platinum NPs (PtNPs), either in pure or alloy form, have been widely used in biomedical applications (Hrapovic et al. 2004). The palladium NPs (PdNPs) are used in catalysis, electro-catalysis, and antibacterial applications (Gopidas et al. 2003). Besides, the non-noble metallic nanoparticles like Fe, Co, Zn, and Se are also being utilized in medical applications, formulations of cosmetic, and antimicrobial applications (Njagi et al. 2011; Lee et al. 2011; Brayner et al. 2006).

With the increasing demand of different metallic and nonmetallic nanoparticles, several physicochemical techniques have been introduced to synthesize NPs with diverse shapes, sizes, and compositions. Both physical and chemical techniques are used to synthesize and stabilize the NPs. Among the different physical techniques, laser ablation (Mafune et al. 2001), lithography, and high-energy irradiation have been used widely throughout the world (Zhang et al. 2008; Treguer et al. 1998), while chemical techniques use chemical reduction or photochemical reduction (Chen et al. 2007; Eustis et al. 2005; Starowiicz et al. 2006). The interaction between the metal ions of the precursors is associated with several parameters like temperature, concentration, and kinetics of the process and the reducing agent, including the adsorption kinetics that helps to stabilize the NPs (Wang et al. 2005).

The toxicity is one of the problems for NPs which arises from the application of hazardous chemical reagents used for preventing the undesirable colloid agglomeration. Besides, some of the NPs are also observed to be toxic caused by the different compositions of metals, shape and sizes, and surface chemistry. This causes toxic NPs unusable in biomedical and clinical applications. However, these influencing parameters can be controlled by using biological mediated techniques, which are environment-friendly and green chemistry-based approaches (Ahmad et al.

2003; Gericke et al. 2006). One of such compounds is chayote, sometimes called *Sechium edule*, which looks like pears with coarse covering and an average length of 10–20 cm (Rao et al. 2017). Several polyphenolic compounds like phenylalanine and tyrosine along with natural antioxidants and amino acids are also the major compositions present in chayote (Sykora et al. 2010). The fruit is rich in flavonoids having 35 mg flavonoids per 10 g of dried chayote fruit and sugar approximately (Rao et al. 2017). The extracts of this fruit showed highly reducing properties and it converts potassium ferricyanide to potassium ferrocyanide (Torres-Chavolla et al. 2010).

In the synthesis of NPs, the metal ions from their corresponding salt precursors are reduced, which results in a color change in the reaction solution during the synthesis of NPs from both the chemical and biological processes. The color change is the first qualitative indication for the formation of NPs. The colloidal nanoparticles in the solution show a Tyndall effect which is used to perceive the existence of the nanoparticles in a solution (Poinern et al. 2013). High-speed centrifugation (~12,000 rpm) is generally used to separate the NPs from the colloid using different advanced techniques. Table 13.1 presents the different techniques for NP synthesis.

13.2 Biological Synthesis of Nanoparticles

The synthesis of NPs from different plants using biological methods is harmless, cheap, and environment friendly (Makarov et al. 2014). Both plants and microorganisms can absorb and build up the inorganic metallic ions from their surrounding environment. The ability of a biological entity in transforming the inorganic metal ions into their respective metal nanoparticles is a comparatively new and largely unexplored technique for NP synthesis (Baker et al. 2013). The ability of microorganisms for the accumulation of metallic ions surrounded in the environments has been exploited in various biotechnological applications like bioleaching and bioremediation processes (Stephen et al. 1999). The interaction capability of the microorganisms with the surrounding environment for oxidation-reduction mechanisms promotes the biochemical conversions. Several studies have shown that both extra- and intracellular synthesis of NPs can also assist them in promoting the redox phenomenon (Mandal et al. 2006). However, the nucleation rate, redox potential, and successive growth kinetics of NPs and their interaction with the metabolic process of microorganisms are yet to be explored (Lengke et al. 2006; Duran et al. 2005). In addition to that, the plants or their extracts have advantages over the other biological based eco-friendly systems like fungi and bacteria, which are needed to take care of the culture preparation or separation techniques. Conversely, due to relatively short production times, plant-based biosynthesis of NPs would be safe and have a negligible cultivation cost than the other living systems (Mittal et al. 2013). Furthermore, plant extract-based biosynthesis addresses a new process that can be easily climbed up to produce NPs in bulk.

Table 13.1 Conventional methods of NP fabrication (Rao 2018)

Fabrication methods	Advantages	Disadvantages
Chemical reduction method	• It was producing AgNPs almost instantly. • Very small particles are formed.	• This method is expensive as the process needs many chemicals as reducing and stabilizing agent.
Chemical vapor deposition	• Produces highly dense and pure materials. • High deposition rate. • Does not require high vacuum. • Low deposition temperature.	• Film deposited at elevated temperature. • Difficult to deposit multicomponent materials. • Use of more sophisticated reactor. • Toxic and corrosive gas generation.
Coprecipitation method	• Low reaction temperature needed. • Impurity level also remains low.	• Needs further grinding and milling to obtain desired NPs.
Bio-mediated synthesis	• Simple, eco-friendly, and energy-efficient synthesis. • Low-cost, non-hazard, and no additional chemicals needed other than metal precursors. • Does not require high temperature and pressure. • Almost free from contamination.	• Prolonged reaction time with some bio-extracts.
Flame spray pyrolysis	• Uniform particle distribution. • High-purity products.	• Raw materials are expensive and highly corrosive. • Controlling size, size distribution, and agglomeration of particles.
Laser ablation methods	• To produce AgNPs without any surface-active agents. • Laser ablation technique in liquid media is simple and efficient and can produce many NPs.	• It has a limitation of NP size control.
Sonochemical	• Very simple, efficient, and additive-free process. • Uniform particle size. • More crystalline in nature.	• More energy consumption.
Sol-gel method	• It is also a low-temperature technique. • Impurity level also remains low.	• Expensive. • Time-consuming process.
Solvothermal method	• This method is useful for synthesizing isotropic nanoparticles. • Particle size is highly controllable.	• Recovery of the product is difficult from the suspension without agglomeration.
Photoreduction	• Simple technique, and fast reaction; within 1–2 h the reaction is expected to complete.	• Expensive process as UV radiation is employed.
Wetness impregnation	• Low processing temperature from 100 to 800 °C. • Easy-to-produce nano-sized particles.	• Some precursor materials are costly. • Collection without aggregation is difficult. • Stoichiometric control can be difficult.

As mentioned above, from many biological substances like bacteria, algae, actinomycetes, plants, fungus, viruses, and yeast the NPs can be synthesized. However, different biological units have enormous skills for the synthesis of metallic NPs or metallic oxide NPs with different degrees of biochemical processing. Enzyme activity can significantly increase under the influence of nutrients, light source, pH of the solution, temperature, mixing speed, and buffer strength (Mukherjee et al. 2001). During the synthesis of NPs, the molecules found in the plant extracts act as both reducing and stabilizing agents (Narayanan and Sakthivel 2008; Sathishkumar et al. 2009); though the biological molecules are chemically complex they are eco-friendly. Different NPs like Co, Pt, and PtCo NPs can be obtained using *S. edule* fruit extract (which contains ascorbic acid) through a bio-mediated process (Rao and Golder 2016). The formation of face-centered cubic (FCC) crystals has been found due to metal ion reduction, and NP destabilization showed intermolecular attractions through conjugation (Tahir et al. 2015).

13.3 Plant Extract-Based Metal Nanoparticle Synthesis

Plants have a high potential biologically to accumulate and reduce the metallic ions (Kulkarni et al. 2014). Due to this property, plants have been considered a more environment-friendly way for biologically synthesizing metallic NPs that are used in detoxification reactions (Khan et al. 2013). Several chemicals like polyphenols, bioactive alkaloids, phenolic acids, proteins, and different other natural products obtained from plant extract play an important role in reducing and stabilizing the metallic ions (Castro et al. 2011). The selection of nanoparticle size and shapes depends on the main contributing factors like composition and concentration of these active biomolecules originated from different plants and their successive interaction between the metal ions in aqueous medium (Li et al. 2011). The synthesis of NPs occurred at room temperature from reducing metal salts via different plant extracts. After mixing the metal salt solution with the plant extract, the process starts, and the biochemical reduction reaction of the salts begins instantly. With the formation of the NPs the appearance of the reaction mixture color changes. Malik et al. (2014) proposed that during the synthesis of NPs, metal ions are oxidized in mono- or divalent oxidation states from their zerovalent states. After that, the smaller neighboring particles merge to form thermodynamically more stable larger NPs under reduction of metal ions that takes place biologically. Akhtar et al. (2013) suggested that nanoparticles are combined to form a variety of morphologies like triangles, spheres, cubes, pentagons, and hexagons. The quality of the synthesized NPs, including size and morphology, is influenced significantly by the properties or composition of the plants' extract. Also, the concentration of metal salt, extract, time of reaction, solution pH, and reaction temperature play a significant role in NP synthesis (Dwivedi and Gopal 2010). Figure 13.1 shows the bioinspired synthesis of Ag/CoNP-Gr using plant extracts.

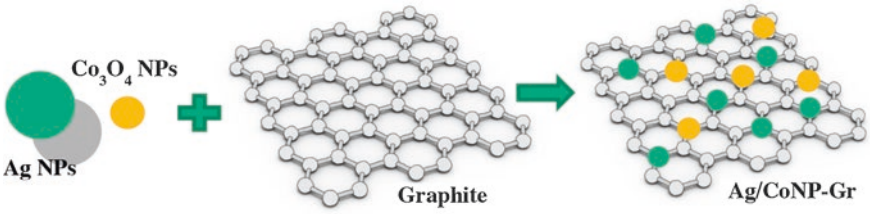

Fig. 13.1 Bio-inspired synthesis of the Ag/CoNP-Gr using plant extracts

13.4 Factors Affecting the Metal Nanoparticle Synthesis

A few controlling factors are involved during the biological synthesis of metallic stabilized nanoparticles. These factors that influence the NP synthesis are solution pH, reactant concentration, time of reaction, and temperature, which are discussed briefly in the subsequent sections.

13.4.1 Influence of pH

During the formation of NPs, the pH plays a significant role during the reaction for the formation of NPs in solution phase (Gardea-Torresdey et al. 1999). Nanoparticles with different shapes and sizes were produced due to the pH variation in the reaction medium. It was observed that at lower pH of the reaction solution, larger particles are produced compared to the particles produced at higher solution pH (Dubey et al. 2010). Armendariz et al. (2004) have suggested that *Avena sativa* biomass was used to synthesize the rod-shaped Au nanoparticles with the particle size in the range of 25–85 nm when synthesized at pH 2. However, the particle sizes are relatively smaller (5–20 nm) when they are synthesized at pH 4. The study reported that more available functional groups are available at pH 4 within the extract to participate in the nucleation process. However, only a few functional groups were available at lower pH value of 2 and led to the particle aggregation and AuNP formation.

In another similar study, *Cinnamon zeylanicum* bark extract has been used to synthesize AgNPs. Also, it has been observed that the number of synthesized particles could be increased with increasing the concentrations of the bark extract. In addition to that at higher pH (>5), the shape of the NPs tended to become spherical (Sathishkumar et al. 2009). On the other hand, at higher pH of the solution the synthesis of palladium (Pd) NPs using *Cinnamon zeylanicum* bark extract showed a slight increment in particle size. The particle size was in the range of 15–20 nm at below 5 of the solution, and at higher pH (>pH 5) the particle size when synthesized was in the range of 20–25 nm (Sathishkumar et al. 2009).

13.4.2 Effect of Concentration

The concentration of the biomolecules significantly influences the formation of metallic NPs. It has been revealed that under the varying concentration of *Cinnamomum camphora* (camphor) leaf extract, the shape of the AuNPs and AgNPs can be controlled (Huang et al. 2007). For example, when the extract concentration of the precursor chloroauric acid was increased, the shape of the resulting NPs was changed from triangular to spherical shape.

13.4.3 Influence of Reaction Time

Ahmad et al. (2012) reported that spherical AgNP synthesis using *Ananas comosus* (pineapple) has occurred within 2 min with a rapid color change. $Ag(NO)_3$ was used and rapidly reduced to Ag^0, and the nanoparticles appeared within 2 min. The produced nanoparticles were spherical in size with a diameter of 12 nm. Dwivedi and Gopal (2010) performed a similar study to produce Ag and Au nanoparticles using different leaf extracts. The formation of nanoparticles started within 15 min of reaction and continued till the next 2 h of reaction. However, the production of NPs was very few beyond the reaction time of 2 h. Prathna et al. (2011) suggested that the reaction time was increased while combining *Azadirachta indica* leaf extract and $Ag(NO)_3$ and also the size of the particles was increased. However, the range was between 10 and 35 nm when the reaction was conducted in 4 h.

13.4.4 Effect of Reaction Temperature

Temperature is an essential factor for the determination of both the size and shape in NP synthesis (Song et al. 2009). For example, when the AgNPs were synthesized using *Citrus sinensis* shell extract at a reaction temperature of 25 °C, the average particle size was around 35 nm. However, when the temperature of the reaction was 60 °C, the average particle size was decreased to 12 nm (Kaviya et al. 2011). Similarly, Song et al. (2009) took *Diospyros kaki* (persimmon) leaf extract for synthesizing AgNPs, and the temperature of the reaction was in between 25 °C and 95 °C. In their study, the particle size was decreased from 110 nm (synthesized at 25 °C) to 40 nm (synthesized at 95 °C). Therefore, by increasing the reaction temperature, the rate of reaction and particle formation appeared to be faster. Though the average particle size was decreased the rate of particle conversion was steadily increased with increasing reaction temperature.

13.5 Green Routes for NP Preparation

13.5.1 AgNPs and Ag-Doped NPs

Plant-based synthesis of NPs is highly favorable due to cost-effectiveness, eco-friendly nature, and their applications in a variety of fields. AgNPs were synthesized from a methanolic extract of *A. marmelos* fruit extract in a greener route. $AgNO_3$ of 1 mM aqueous solution was prepared for the synthesis of AgNPs. Co-precipitation technique using the fruit extract of *A. marmelos*, a reducing and plugging agent, was employed to synthesize the AgNPs from $AgNO_3$ solution (Devi et al. 2019). When the formation of NPs starts the color of the reaction solution changes as shown in Fig. 13.2. The bio-reduction of Ag^+ with the wavelength range from 350 to 680 nm in aqueous solution was detected using a UV spectrophotometer. To discover the mechanistic pathways of the reduction of Ag metal ions from its corresponding salt, the extract of the fungus was dialyzed for 42 h at 4 °C against distilled water. Then 200 µL of 20 mM nicotinamide adenine dinucleotide phosphate (NADPH) was mixed with 10 mM $AgNO_3$ solution (Boulch et al. 2001).

Moreover, the doped NPs are also becoming popular as they have multifunctional properties. Recently, Nigussie et al. (2018) have reported the Ag-doped TiO_2 synthesized using $TiCl_4$ combined with ethanol under continuous stirring. Then $AgNO_3$ was mixed gently with 0.5 mL deionized water (DI) to form gelation precipitation of AgNPs and dried at 100 °C for 24 h. The amorphous TiO_2 transformed into a crystalline structure using 460 °C for 5 h. Ag-doped ZnO nanopowder was also synthesized with a similar path using $AgNO_3$ which was added to the zinc solution containing NaOH solution, and then $Ag(OH)_2$ was formed as a precipitate. The Ag-doped ZnO NPs were obtained, and the powder was then calcined in an atmospheric air for 7 h at 460 °C (Nigussie et al. 2018).

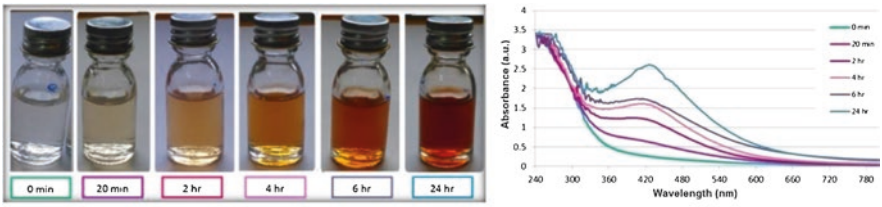

Fig. 13.2 Change in solution color (**a**) and change of absorbance (**b**) in UV-vis spectra with the formation of AgNPs (Erjaee et al. 2017)

13.5.2 Zerovalent Iron NPs and Fe-Doped NPs

In various fields of medical science, the iron-based nanomaterials have shown a wide application in treating ecological pollution (Tripathi and Chunga 2019). Zerovalent iron nanoparticles (FeNPs) have been used in the field of biodegradation for the removal of different heavy metals like Hg, Ni, Cd, Pb, and Cr. The Fe^0 NPs can also be synthesized using the microbial biomasses or plant extracts. Mehrotra et al. (2017) showed that *yeast* extract has been used to synthesize the FeNPs. The solution of *yeast* extract was prepared by dissolving 2.0 g of *yeast* powder in 25 mL of deionized water followed by continuous boiling for 15 min (Tripathi and Chunga 2019). Ferric chloride ($FeCl_3$, 1 mM) solution was used as a source of Fe^{3+} ions for the reduction of Fe^{3+} ions to Fe^0 by dissolving about 750 μL of *yeast* extract solution in it. With the continuous development of the NPs, the color of the solution was transformed rapidly from light yellow to brown, indicating the formation of FeNPs.

13.5.3 AuNPs and Au-Doped NPs

Gold nanoparticles (AuNPs) attracted researchers due to their optical properties. Its colloidal solutions can be obtained by the reduction of Au(III) nanoparticles (Sun et al. 2017). The newly formed AuNPs in red color have surface plasmon resonance absorption (Sun et al. 2017). In addition, ligand-exchange reactions with functionalized molecules play an important role in the synthesis of optical materials and sensors from AuNPs (Zhang et al. 2012), catalysts (Deparis et al. 2009), etc. Recently, NPs have been prepared from different tea extracts. In green and black tea extracts both reductant and surfactant are present; they have been used in the "green" research of metal NPs (Cha et al. 2000; Zhou et al. 2014).

The NPs can be synthesized using green tea extract by using green tea leaves with 100 g to 750 mL of water and allowing this mixture in the refrigerator for 24 h at ~0 °C. About 500 mL of water was added to the tea extracts after filtration under identical conditions. An aqueous solution of 10 mM $HAuCl_4$ is then added to a solution of 900 μL tea extract at ambient temperature, having a metal concentration of 1 mM of AuNP solution. Das et al. (2011) have synthesized spherical shaped AuNPs using *Nyctanthes arbortristis* (night jasmine) flower extract ranging from 7 to 55 nm. The diverse shapes of decahedral, triangular, and spherical have been shown in the synthesized particles (Narayanan and Sakthivel 2008). Au/TiO_2 NPs can be produced from AuNP solution by mixing with 40 mM of TiF_4 with a continuous stirring followed by isolated Au/TiO_2 NPs having core-shell-like structure using centrifugation at 6000 rpm for 8 min (Sun et al. 2017). Coupling between TiO_2 and NPs, which are made by noble metal, has been used as an effective approach to overcome these walls (Zhang et al. 2012; Jiang et al. 2014).

13.5.4 CuO- and Cu-Doped NPs

CuNPs and copper-copper oxide (Cu/CuO) have been produced from Magnolia leaf extract ranging from 45 to 100 nm (Lee et al. 2011). CuNPs spherical in shape having the potential of antibacterial activity against *E. coli* cells are produced by a green route from *Syzygium aromaticum* (clove) extracts with a mean particle size range of 40–55 nm (Subhankari and Nayak 2013). An average particle size of cuprous oxide NPs was 4.8 nm that has been formed from the *Sterculia urens* (karaya gum) extract which has the ability to synthesize highly steady spherical NPs (Padil and Cerník 2013). The particles have been found to be effective in antimicrobial activity tests against common pathogens like *E. coli* and *Staphylococcus aureus*. Das et al. (2013) have also observed that both antioxidant and antibacterial behavior was found in CuONPs.

13.5.5 Mixed Metal/Metal Oxide NPs

Several metal oxide NPs such as titanium dioxide (TiO_2), zinc oxide (ZnO), and palladium oxide (PdO) nanoparticles with an effective size range from 100 to 150 nm have been reported using green route (Roopan et al. 2012). An extract from *Psidium guajava* was used to produce TiO_2 nanoparticles that have both antibacterial and antioxidant properties, which are estimated against *Aeromonas hydrophila*, *Proteus mirabilis*, and *E. coli* (Santhoshkumar et al. 2014). The antibacterial and antioxidant properties of TiO_2 were found to be most effective against *E. coli* and have also been observed and found to be harmful to several bacterial strains (Heinlaan et al. 2008).

The ZnO nanostructure shows high electron/hole (e^-/ h^+) binding energy (60 meV) with a wide bandgap (3.37 eV) (Mitra et al. 2012). ZnO NPs have been used in various fields of applications like in optical devices (Yude et al. 2006), biosensors (Hwa and Subramani 2014), solar cells (Al-Kahlout 2015), and photocatalysis devices (Tripathi et al. 2014). Rao et al. (2018) have synthesized Ag-doped ZnO using the analyte ascorbic acid (294 mg per kg fruit) extracted from *Sechium edule* in aqueous solution. The bandgap of ZnO was decreased to 2.85 eV from 3.13 eV at the optimum Ag loading with 1.18% (w/w) under the control catalytic system as shown in Fig. 13.3, while the commercial analyte ascorbic acid can diminish the bandgap up to 2.91 eV (Rao et al. 2018).

13.6 Characterization Techniques of NPs

The different techniques such as UV-vis spectroscopy, transmission electron microscopy (TEM), dynamic light scattering, X-ray powder diffraction, energy-dispersive spectroscopy, diffuse reflectance spectroscopy, and zeta potential are used for

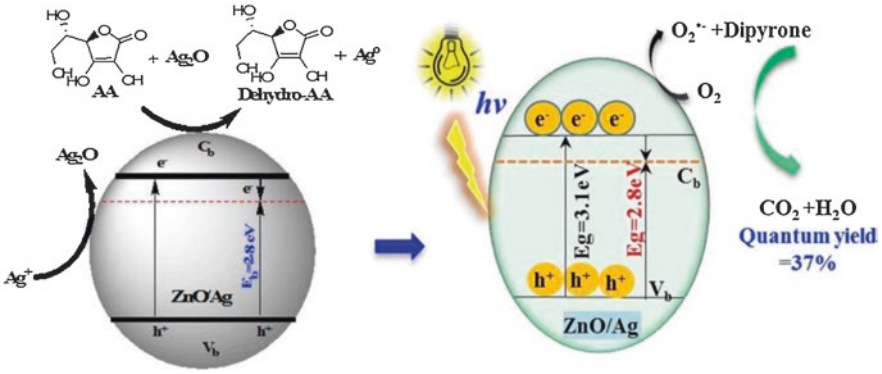

Fig. 13.3 Ag-doped ZnO supported by an ascorbic acid used as a potential bio-analyte rich for photocatalytic degradation of dipyrone drug (Rao et al. 2018)

characterizing the NPs. The detailed discussion is given below for the NP characterization.

13.6.1 UV-Vis Spectroscopy Method

The bandgap energy of any NPs can be determined by UV-visible absorption spectroscopy. For example, Co_3O_4 NPs were measured by UV-vis. The bands were found to be at 600–800 nm and 350–600 nm for their corresponding O^{2-}-to-Co^{3+} and the O^{2-}-to-Co^{2+} charge transfer transitions, respectively (Das et al. 2017). The corresponding bandgaps have been found to be 1.42 and 2.53 eV (Sharma et al. 2015). The absorption peaks of Co_3O_4 NPs are observed at 427 nm and 739 nm (Naveen and Selladurai 2015). Melissa et al. (2013) suggested that the photocatalytic-reactive oxygenated species (ROS) produced by metal oxide NPs have been detected, where TiO_2 or ZnO with the wide-bandgap semiconductors produced electron (e^{-1})/hole (h^+) pairs causing redox reaction under UV light irradiation.

Also, UV-visible absorption spectroscopy helps to identify the formation of different-sized NPs. In the case of variation in solution pH, the formation of AgNPs also changes, and accordingly the solution color also changes when synthesized with different pH (viz. pH 3–12.5). The variations of both color change of the reaction mixture and its optical absorbance at different pH are shown in Fig. 13.4. At pH 1, absorbance peak did not appear within the whole range of the wavelength because of no AgNP formation. However, with a gradual increase in pH the absorption peak visibility was increased. Rao and Golder (2016) observed a minor peak at a wavelength of 428 nm and pH 3 when AgNPs were synthesized. By increasing the peak intensity, the absorption was shifted to lower wavelengths up to 414 nm when synthesized at pH 12.5 as shown in Fig. 13.4. Smitha et al. (2008) suggested that the AgNP shows some characteristic peaks in the suspension obtained from shape- and

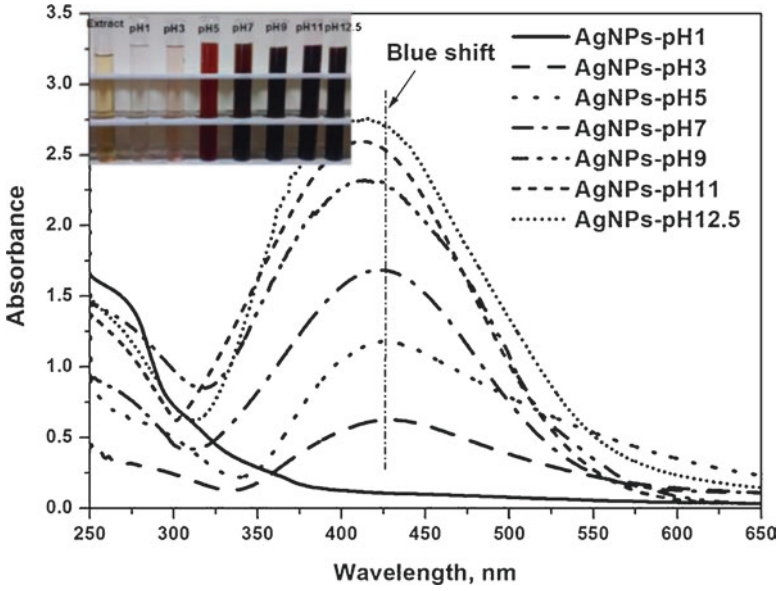

Fig. 13.4 Spectral absorbance of $AgNO_3$ and bio-extract mixture at different pH (Rao et al. 2016)

size-dependent surface plasmon resonance (SPR) effect. This reduction in the size and/or degree of anisotropy of the particles is indicated by the hypsochromic shift (Edison and Sethuraman 2013; Yilmaz et al. 2011). AgNPs show a very minute change in the color of the solution after 24 h of reaction time. The color was changed by increasing the pH from light red-brown to dark red-brown, as shown in Fig. 13.4 (inset). The conversion rate from Ag^+ to Ag^0 in AgNPs was faster with increasing pH at the initial period (Rao and Golder 2016). It has been found that about 88.5% of Ag^+ was converted to Ag^0 present in AgNP solution at pH 12.5 within 12 h. It was increased up to 96% when the reaction mixture was kept for 24 h. In another study, the UV-visible spectrum of the NiO-NPs has been dispersed in water existing at the wavelength of 319 nm with a strong band that may be caused by the presence of NiO-NPs. This is attributed to the electronic transition in $O_{(2p)}$ of the valence band to $Ni_{(3d)}$ of the conduction band in the NiO semiconductor (Barakat et al. 2013). Al-Sehemi et al. (2014) reported that the bandgap energy of the NiO-NPs was about 3.55 eV from the UV-vis spectroscopy experimentation.

13.6.2 Dynamic Light Scattering of NPs

The average particle size or size distribution has been found to be dependent significantly on the properties of the NPs, and this can be analyzed using the dynamic light scattering (DLS) analysis. A representative result of AgNPs is shown in Fig. 13.5.

From Fig. 13.5, it can also be observed that the particle size distribution is directly influenced by the solution pH. As the solution pH increases, the particle size becomes smaller. Rao and Golder (2016) have reported that the lowest and the highest particle size distribution was found to vary from 51 to 193.9 nm and 7.1 to 10.9 nm for AgNPs at pH 3 and pH 12.5, respectively. In another study by Rao and Golder (2019), it has been found that the hydrated layer of the organic molecules present on the surface of NPs is 60% greater than the hydrodynamic diameter of PtNPs, CoNPs, and PtCo (1:1) NPs. The change of the zeta potential was counted by the DLS analysis (Kuehner et al. 1997). The PtNPs showed the maximum mass loss due to smaller particle sizes (42.62 nm) with a high surface area surrounded by a more covering agent (Table 13.2).

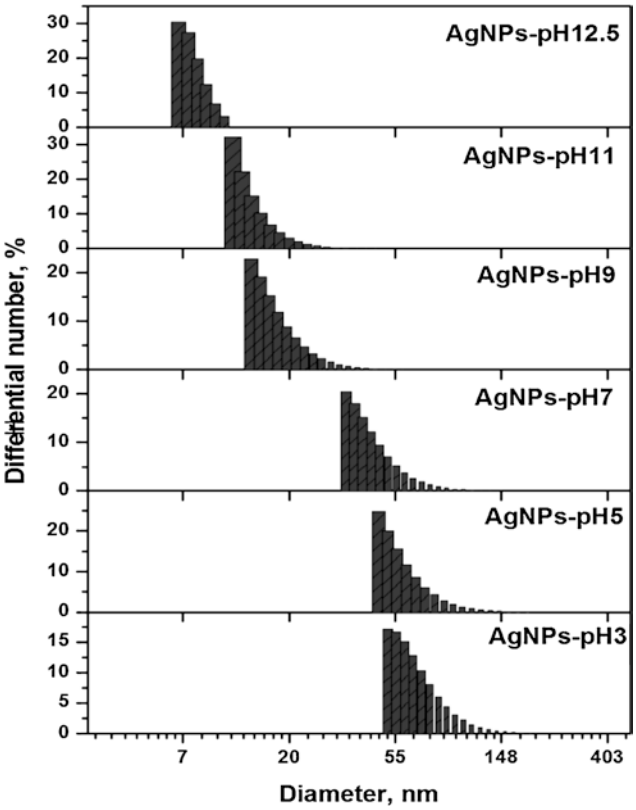

Fig. 13.5 Particle size distribution by dynamic light scattering with pH variation during AgNP synthesis (Rao et al. 2016)

Table 13.2 Characteristic parameters of AgNPs synthesized at different pH (Rao et al. 2016)

Sample	UV-vis absorption		Particle size calculated from XRD data		Particle size calculated from DLS data		Particle size calculated from TEM		Particle size calculated from FESEM	
	SPR peak (nm)	FWHM	d-Spacing (nm)	Crystallite size (nm)	Mean size	Size range	Mean	Size range	Mean	Size range
AgNPs at pH 3	428	168.7	0.23591	54.069	68.2	51–194	57.31	20–110	58.56	20–110
AgNPs at pH 5	427	146.9	0.2354	35.159	60.1	47–189				
AgNPs at pH 7	424	136.6	0.2354	34.479	44.9,	34–131				
AgNPs at pH 9	417	116.9	0.2354	22.247	31.2	14–58	25.94	5–50	25.37	5–50
AgNPs at pH 11	416	113.7	0.23543	22.344	14.5	12–44				
AgNPs at pH 12.5	414	108.9	0.23537	20.716	8.9	7–11				

13.6.3 TEM and FESEM Study

The surface morphology of the NPs can be measured by the SEM and TEM analysis. For example, Das et al. (2017) have used the SEM micrographs of Co_3O_4 to investigate the detailed surface morphology of Co_3O_4 NPs. They have also reported that Co_3O_4 NPs were mostly present in an irregular aggregate manner due to the presence of grain boundaries with a weak migration and a significant number of amorphous phases. The sizes of the Co_3O_4 NPs are normally in an average diameter of 20.8 nm and the size range varies from 5.8 to 38.1 nm.

The orientation of crystallites of Co_3O_4 at 500 °C for 12 h was found to be increased due to more distinct grain boundaries and the agglomeration of small grains shows the increase in average particle size to 28.12 nm. Rao and Golder (2016) have reported that the shape, size, and morphology of AgNPs were determined using TEM and FESEM analysis at pH range from 3 to 12.5, and the results are presented in Table 13.2. AgNP size was more substantial with a significant agglomeration at pH 3. However, at pH 9, the small particles of AgNPs were mostly separated, and the agglomeration was found to be reduced.

The interplanar spacing and lattice plane can also be measured from TEM analysis. A clear lattice boundary in a single AgNP with an interplanar d-spacing of 0.2354 and 0.236 nm was found by high-resolution TEM micrograph at pH 3 and pH 9, respectively (Rao and Golder 2019). The similar studies can also be

Table 13.3 Determination of particle sizes of PtCo mono- and bimetallic NPs (Rao et al. 2019)

	Calculated from FESEM analysis		Calculated from TEM analysis		Calculated from DLS analysis		Calculated from XRD analysis	
NP sample	Mean (nm)	Size range (nm)	Mean (nm)	Size range (nm)	Mean	Size range	d-Spacing (nm)	Crystallite size (nm)
Pt	28.76	10–70	–	–	43.62	10–122	0.2296	22.19
Co	47.55	40–110	–	–	69.00	21–143	0.2128	35.16
PtCo (1:1)	25.11	10–80	27.9	10–80	60.12	14–172	0.2248	32.08

performed to determine the d-spacing from XRD analysis as shown in Tables 13.2 and 13.3 (Rao and Golder 2016; Rao and Golder 2019). Sun et al. (2017) have shown that the TEM image of Au/TiO_2 shell-like NPs was made at 100 °C under an identical condition. Comparing with the shell-like NPs synthesized at 180 °C, the same NPs synthesized at 100 °C showed thicker shell width of 32 nm. The average diameter of 50 nm of the hollow structure of each AuNP appears as light gray thin shells that have also been verified by TEM image (Tu et al. 2015). Figure 13.6 shows the different morphological shapes of NPs using SEM analysis (Elechiguerra et al. 2006).

13.6.4 Influence of Zeta Potential (ζ)

The zeta potential basically shows the study of the stability of the NPs. Malika et al. (2016) have studied the destabilization tendency of NPs in aqueous media using zeta potential (ζ) analysis. Zhang et al. (2009) showed that the adsorption of biomolecules generally shows a negative surface charge due to the formation of AgNP-ascorbate layer. Zeta potential was inversely changed with pH from 3 to 12.5 and was found to be decreased from −3.8 to −25.8 mV between pH 3 and 11 (Rao and Golder 2016). It suggests that the higher pH of the reaction helps to achieve stable AgNPs (Fig. 13.7). Moreover, by increasing the pH the concentration of silver-ascorbate layer is increased which leads to the formation of nanocrystal surface (Oluwafemi et al. 2010). The change in ζ was measured in aqueous colloidal medium of PtNPs and CoNPs and was found to be negative for all metal NPs. These NPs were originated from different biomolecules such as ascorbate layer obtained from ascorbic acid acting as the formation of NP-ascorbate layer. The ζ was gradually reduced from −3.2 to −37.1 mV with increasing pH from 3 to 12 in the case of PtNPs. The ζ for CoNPs was decreased from −3.2 to −31.1 mV when pH reduced from pH 3 to pH 12. Similarly, the ζ for PtCo bimetallic NPs was changed from

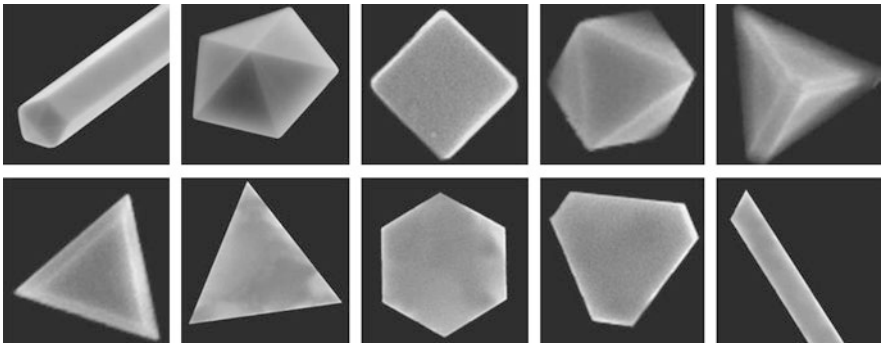

Fig. 13.6 Different morphologies of particles: nano-wire pentagonal shape, decahedral shape, cubic shape, octahedral shape, tetrahedral shape, truncated tetrahedral shape, and platelet shape (Elechiguerra et al. 2006)

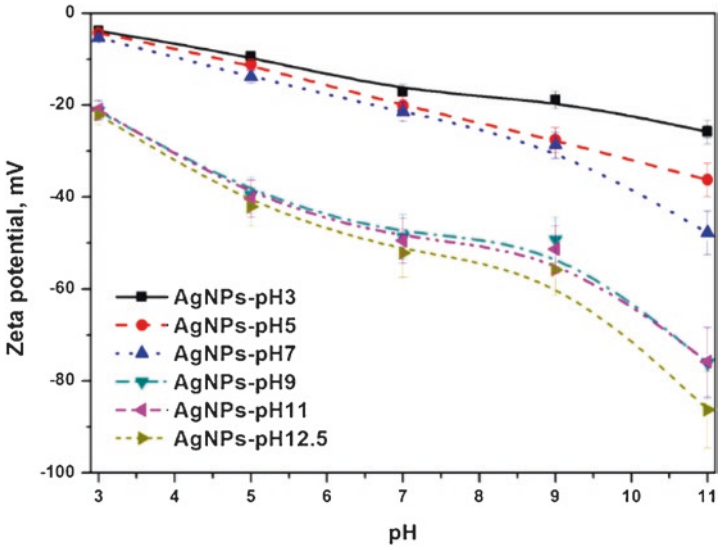

Fig. 13.7 Zeta potential of synthesized AgNPs with pH variation (Rao et al. 2016)

−5.1 mV at pH 3 to −46.2 mV at pH 12.5. The higher negative value of ζ shows the repulsion of the particles and helps to remain as an individual unit in a suspension. It is recommended that the bimetallic NPs like PtCoNPs act as an efficient catalyst compared to the monometallic NPs.

13.6.5 Structural Morphology

The crystalline structure of the NPs can be estimated using XRD data. The average particle size can also be determined using Scherrer's formula. Rao and Golder (2016) have synthesized AgNPs and calculated the crystallite size for the samples synthesized at different pH values (Fig. 13.8). Zuas et al. (2014) showed that the major peaks for an FCC crystal of AgNPs at 2θ value of 38, 46, 65, and 78° attributed to the lattice plane of (111), (200), (220), and (311), respectively. Rao and Golder (2016) reported a reduction in crystalline size due to the peak expansion from 54.1 nm to 21.7 nm for AgNPs at pH 3 and pH 12.5, respectively, during its formation. However, with pH variation (Table 13.2) the d-spacing did not change between the adjacent lattice planes. AgNPs were synthesized with a minor peak at $2\theta = 32.2^{o}$ at pH 3, indicating the existence of Ag_2O. Therefore, XRD analysis of AgNPs clearly showed the bi-crystalline structure for both samples synthesized at low as well as higher pH. AgNPs were synthesized from tea leaf extract and similar results have also been found (Sun et al. 2014). The average size of the CuNPs has been found to be 13.13 nm with a space group of pccn (56) and maximum peak intensity at 2θ value of 42.045 (Chaudhary et al. 2019). Chaudhary et al. (2019) also suggested the maximum intensity of the NiNPs of diffraction peak at 2θ = 12.50 with the size of 24.0 nm which indicates the presence of crystalline structure. The average grain size obtained from the XRD pattern of Au/TiO_2 NPs synthesized at 100 °C was calculated using the Scherrer's formula from the half-width of the anatase main (101) diffraction peak (Zhong et al. 2010). Sun et al. (2017) have

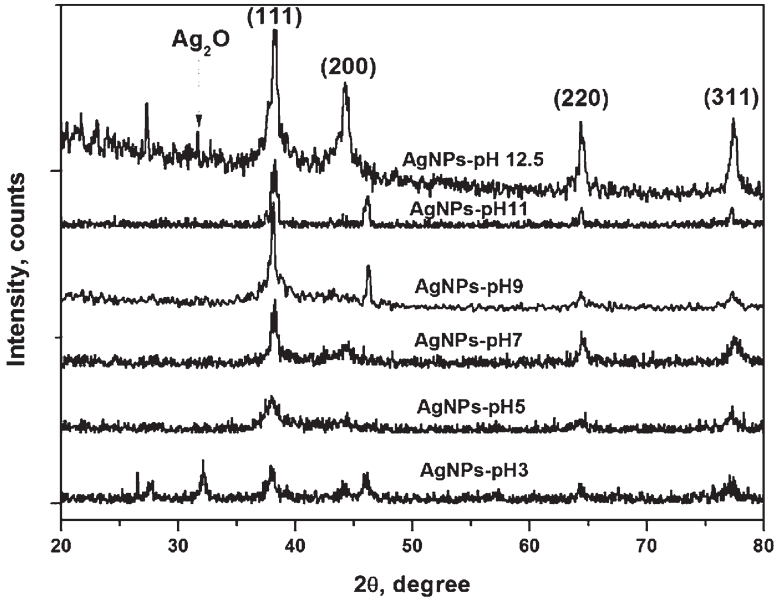

Fig. 13.8 XRD patterns of synthesized AgNPs (Rao et al. 2016)

estimated the Au/TiO_2 NP size as 14.2 nm and 12.6 nm for synthesizing at 180 °C and 100 °C, respectively. It is a sign of grain growth and the thinner shell appeared when synthesized at high temperature (Sun et al. 2017).

13.7 Mechanism of NP Formation Using Bio-extract

The synthesis of AgNPs using guava leaf extract has been described in this section as a representative mechanism of NP synthesis through bio-extract. The mechanism is as follows:

Chlorogenic acid derivative (dimethoxy cinnamoylquinic acid), D-glucose, and quercetin are the major constituents present in *P. guajava* leaves (Fierascu et al. 2017). AgNPs originated from Ag^+ which get reduced to Ag^0 forming silver nuclei, while the corresponding leaf components are oxidized to form CO_2 and H_2O as ultimate products along with other daughter ions as shown in Fig. 13.9. Glucose molecule with MW = 180 takes part in AgNP formation along with the other product P_4 (MW = 118.20). Then Ag^+ forms a complex (P_1) with MW 283.09 in the presence of deprotonated glucose molecule (β-D-glucopyranoside) under an alkaline medium (pH = 9.5) (Chakraborty et al. 2017) and oxidizes to acid (P_2, MW = 197.03). This is further converted to P_4 after decarboxylation reaction of P_2 followed by dihydroxylation of P_3 molecule (MW = 152.11). Hence, Ag^+ is coordinated with hydroxyl groups (-OH) (Baksi et al. 2015):

$$2Ag^+ + 2OH^- \rightleftarrows 2AgOH \leftrightarrow Ag_2O + H_2O \tag{13.1}$$

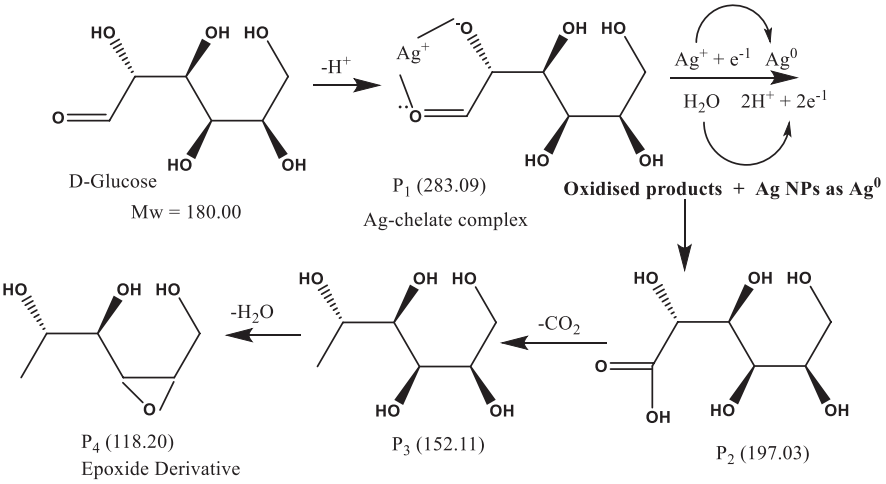

Fig. 13.9 Plausible mechanism of AgNP formation in the presence of D-glucose (present in guava leaf extract)

$$C_6H_8O_6 + Ag_2O \xrightarrow{OH^-} 2Ag^0 + C_6H_7O_6^{\bullet -} + H_2O \quad (13.2)$$

$$2C_6H_7O_6^{\bullet -} + Ag_2O + H^+ \rightarrow \text{Ascorbate anion} + \text{dehydro} \quad AA + 2Ag^0 + H_2O \quad (13.3)$$

Bachmann et al. (2014) suggested that *S. edule* extract was used to produce dehydro-AA through a free radical intermediate originated from ascorbic acids (AA) at mild acidic and neutral pH in a reversible process (Eqs. 13.1–13.3). However, the higher pH shows an irreversible interconversion (Wechtersbach and Cigic 2007). Figure 13.8 shows a mechanistic route of interconversion of Ag^+ to Ag^0 for the formation of AgNPs. Glucose molecule as a sacrificial electron donor reduces Ag_2O (or Ag^+) and P_1 (m/z 283.09) followed by the formation of Ag-glucose chelate complex. After that, a fragment with P_2 (m/z 197.03) is formed on the cleavage of Ag-glucose complex, and simultaneously Ag^+ is reduced to Ag^0. The fragment P_3 with molar mass 152.11 g/mol is converted to an epoxide compound P_4 having m/z 118.20 through decarboxylation ($-CO_2$) reaction. This epoxide intermediate may be converted to oxalic acid, xylosone, and xylonic acid (Zhang et al. 2014).

13.8 Antimicrobial Activity Test of NPs

Among the various applications, NPs can also be used for the inhibition of bacteria. Saravanakumar et al. (2017) have employed various bio-inspired Ag-based NPs for their antibacterial activity including the NPs of Cu Pd (Surendra et al. 2016), Pt (Tahir et al. 2015), ZnO (Vijayakumar et al. 2018) (Lv et al. 2017), and Fe_2O_3 (Arokiyaraj et al. 2013). The antibacterial activity of biosynthesized AgNPs using *Ficus benghalensis* revealed that AgNPs with a concentration of 45 μg/mL showed the potential antibacterial activity with a minimum inhibitory concentration of 25 μg/mL (Tripathi and Chunga 2019; Saxena et al. 2012). The antibacterial activity of AgNPs has shown bacterium resistance to common antibiotics (Salomoni et al. 2017). Lv et al. (2017) have investigated the antibacterial activity of CuNPs and found that 100 μg/mL of CuNPs is required to have an effective antibacterial activity with the 10^5 CFU/mL *E. coli* suspension within 12 h (Lv et al. 2017). The biosynthesized PdNPs having the particle size of 27 nm with spherical shape exhibited a good antibacterial activity against *Staphylococcus aureus* and *E. coli* (Surendra et al. 2016). Tripathi et al. (2018) have investigated biogenic AgNPs to develop polyvinyl alcohol (PVA) used for food packaging materials and it also acts as an antibacterial biodegradable nanocomposite film (Tripathi et al. 2018). The bacterial growth inhibition experiment in the presence of AgNPs has been tested at pH 9 using two bacterial strains, i.e., *B. subtilis* and *E. coli*, and it has been observed that the rate of inhibition gradually increased with increasing particle concentration (Rao and Golder 2016). The potential toxicity may be altered by the different iron-based NPs due to their interactions with inorganic/organic contaminants. Iron-based

NPs (Fe_2O_3 NPs) due to their excellent adsorption properties may act as a carrier to transfer the target contaminants into cells (Hu et al. 2012). The toxicity of zerovalent iron NPs (Fe^0NPs) is a progressiveness of test organisms, function of their properties, and ecological conditions. They have been more considered in the field of water and wastewater remediation due to their adsorption-desorption efficiency. But at the same time, it is also becoming a source of NP contamination in the environment. NPs made by zerovalent iron reduce the concentrations of solvents nearly to zero within days, and at the same time, due to a significant change in oxygen levels, the pH level was also reduced (Fuhrer et al. 2000).

In additional information reported by Sadiq and Chandrasekaran (2010), TiO_2 nanoparticles with 20 nm diameter have been used for toxicity test to *E. coli, P. aeruginosa*, and *B. subtilis* through membrane damage under non-illuminated conditions. The production of reactive oxygen species (ROS) by the UV light irradiation and the existing rate of *E. coli* on ZnO, TiO_2, Al_2O_3, CeO_2, and Fe_2O_3NPs may have contributed to toxicity (Li et al. 2012). It has been observed that CuO microparticles have higher toxicity compared to CuONPs (Nutt et al. 2005). Likewise, the TiO_2NPs produced more DNA damage capacity compared to the ZnONPs (Wang and Zhang 1997). The toxicities of Ag, Ag, and Fe_3O_4NPs have been considered on plants and microorganisms (Elliott and Zhang 2001; Liu et al. 2005). Rao and Golder (2016) investigated the biological activity of both AgNPs and aqueous bio-extract and their results have been linked with the control media. An inactivation study of *B. subtilis* and *E. coli* bacteria has been chosen for the two antibiotics streptomycin and ampicillin, respectively. AgNPs exhibited the zone diameter of 22 mm with the lower inhibition of *B. subtilis,* while AgNPs showed to be most effective to suppress the growth of *E. coli* with 36 mm zone diameter of inhibition (Rao et al. 2017). This is explained by the extent of variation of permeability of AgNPs to the bacterial cell wall and the difference in the rate of growth inhibition for both gram-negative and gram-positive bacteria. A defensive peptidoglycan layer in outer membrane has been observed for the gram-negative bacteria, while gram-positive organisms do not have this (Li et al. 2009). Adegboyega et al. (2013) reported that AgNPs might cross the permeability barrier of the external membrane with free radical resulting in the seepage of cellular materials. Therefore, the disorder of membrane permeability could play a significant role in the inhibition of bacterial growth by AgNPs (Adegboyega et al. 2013). An antimicrobial activity of AgNPs for both types of bacterium growth is addressed in Fig. 13.10.

13.9 Overview

This chapter discussed the cost-effective and eco-friendly procedures for different NPs' synthesis by utilizing a natural resource, i.e., varieties of fruits and leaf extracts, which are excellent reducing agents, including the use of biological entities for the synthesis of metal and metal-doped nanoparticles discussed in detail. The potential of metal-metal oxide nanoparticles produced in different greener routes

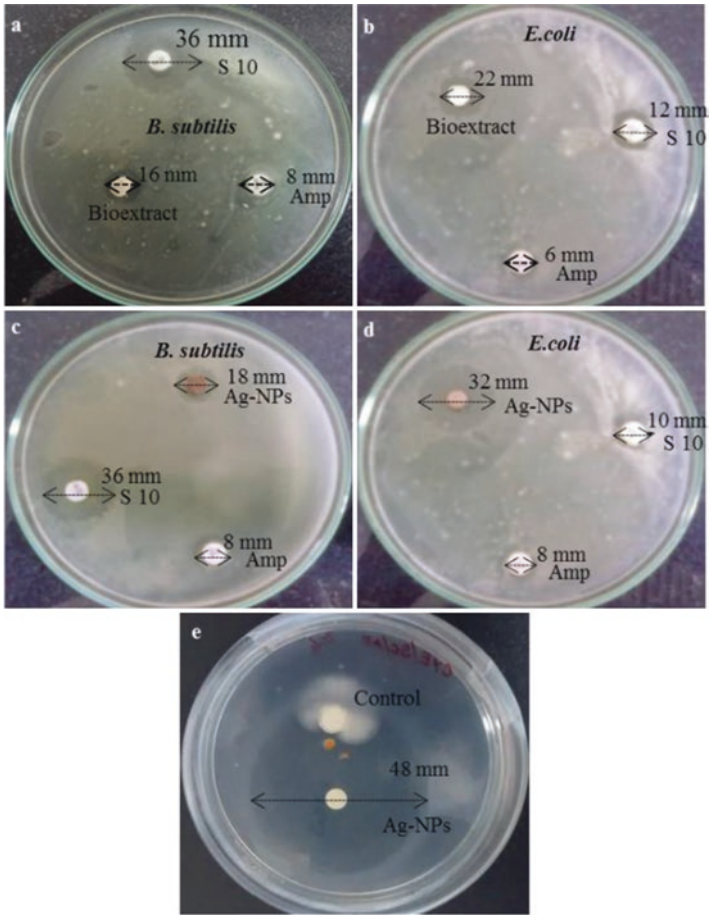

Fig. 13.10 Illustrative image showing AgNPs and their inhibiting growth of *B. subtilis* (**a**, **c**) and *E. coli* (**b**, **d**) in an antibiotic control media. (**e**) Antifungal activity of chayote extract against *Aspergillus thermomutatus* (Rao et al. 2017)

has been showing a significant interest in various areas like medicine, agriculture, and electronics. The biological things help to attain stable, cost-effective, nontoxic, and environment-friendly NPs through the green chemistry approach. The bio-inspired synthesis of NPs from various aqueous bio-extracts is strongly pH dependent, which may also play a role in determining the size, shape, stability, and purity of particles. At synthesized pH 3, 7, and 12.5, the corresponding diameters of NPs were found to be 68, 45, and 12.5, respectively. The higher pH facilitates the prevention of particle aggregation due to formation of a metal-ascorbate layer on NPs and the intense negative zeta potential. The NPs have a potential property in inhibiting the bacterium growth like *E. coli, B. subtilis,* and *P. aeruginosa*. In fact, NPs are synthesized through different bio-inspired methods for developing antibacterial

biodegradable nanocomposite film for food packaging materials. The use of plant extracts for the synthesis of NPs is inexpensive and environmentally friendly, and can be scaled up easily. More interestingly, the plant extracts have the potential of producing NPs with the specific shape, size, or composition.

References

Adegboyega NF, Sharma VK, Siskova K, Zboril R, Sohn M, Schultz BJ, Banerjee S (2013) Interactions of aqueous Ag1 with fulvic acids: mechanisms of silver nanoparticle formation and investigation of stability. Environ Sci Technol 47:757–764

Ahmad A, Senapati S, Khan MI, Kumar R, Sastry M (2003) Extracellular biosynthesis of monodisperse gold nanoparticles by a novel extremophilic actinomycete, Thermomonospora sp. Langmuir 19(8):3550–3553

Ahmad N, Sharma S (2012) Green synthesis of silver nanoparticles using extracts of *Ananascomosus*. Gr Sustain Chem 2(4):141–147

Akhtar MS, Panwar J, Yun YS (2013) Biogenic synthesis of metallic nanoparticles by plant extracts. ACS Sustain Chem Eng 1(6):591–602

Al-Kahlout A (2015) Thermal treatment optimization of ZnO nanoparticles-photoelectrodes for high photovoltaic performance of dye-sensitized solar cells. J Assoc Arab Univ Basic Appl Sci 17:66–72

Al-Sehemi AG, Al-Shihri AS, Kalam A, Du G, Ahmad T (2014) Microwave synthesis, optical properties and surface area studies of NiO nanoparticles. J Mol Struct:56–61

Armendariz V, Herrera I, Peralta-Videa JR, Jose-Yacaman M, Troiani H, Santiago P, Gardea-Torresdey JL (2004) Size controlled gold nanopartilce formation by Avena sativa biomass: Use of plants in nanobiotechnology. J Nanopart Res 6(4):377–382

Arokiyaraj S, Saravanan M, Prakash NU, Arasu MV, Vijayakumar B, Vincent S (2013) Enhanced antibacterial activity of iron oxide magnetic nanoparticles treated with Argemone mexicana L. leaf extract: an in vitro study. Mater Res Bull 48:3323–3327

Asha Rani PV, Kah LG, Hande MP, Viliyaveettil S (2009) Cytotoxicity and Genotoxicity of silver nanoparticles in human cells. ACS Nano 3(2):279–290

Bachmann C, Probst B, Guttentag M, Alberto R (2014) Ascorbate as an electron relay between an irreversible electron donor and Ru(II) or re(I) photosensitizers. Chem Commun 50:6737–6739

Baker S, Harini BP, Rakshith D, Satish S (2013) Marine microbes: Invisible nanofactories. J Pharm Res 6(3):383–388

Baksi S, Zhenli l, Willie GH (2015) Natural nanoparticles: implications for environment and human. Health Environm Sci Technol 45:861–904

Barakat A, Al-Noaimi M, Suleiman M, Aldwayyan AS, Hammouti B, Hadda TB, Haddad SB, Boshaala A, Warad I (2013) One step synthesis of NiO nanoparticles via solid-state thermal decomposition at low-temperature of novel aqua(2,9-dimethyl-1,10 phenanthroline)$NiCl_2$ complex. Int J Mol Sci 14(12):23941–23954

Boulch F, Schouler MC, Donnadieu P, Chaix JM, Djurado E (2001) Domain size distribution of YTZP nanoparticles using XRD and HRTEM image. Anal Stereol 20:157–161

Brayner R, Ferrari-Iliou R, Brivois N, Djediat S, Benedetti M, Fiévet F (2006) Toxicological impact studies based on Escherichia coli bacteria in ultrafine ZnO nanoparticles colloidal medium. Nano Lett 6(4):866–870

Castro L, Blazquez ML, Munoz JA, Gonzalez F, Garcıa-Balboa C, Ballester A (2011) Biosynthesis of gold nanowires using sugar beet pulp. Process Biochem 46(5):1076–1082

Cha JN, Stucky GD, Morse DE, Deming TJ (2000) Biomimetic synthesis of ordered silica structures mediated by block copolypeptides. Nature 403:289–292

Chakraborty S, Rao CV, Das RK, Giri AS, Golder AK (2017) Bio-mediated silver nanoparticle: synthesis mechanism and microbial inactivation. Toxicol Environ Chem 99(3):434–447
Chaudhary J, Tailor G, Kumar D, Joshi A (2017) Synthesis and thermal properties of copper nanoparticles. Asian J Chem 29(7):1492–1494
Chaudharya J, Tailora G, Yadav BL, Michael O (2019) Synthesis and biological function of Nickel and Copper nanoparticles. Heliyon 5(6):e01878
Chen ZH, Jie JS, Luo LB, Wang H, Lee CS, Lee ST (2007) Applications of silicon nanowires functionalized with palladium nanoparticles in hydrogen sensors. Nanotechnol 18(34):345502
Daniel MC, Astruc D (2004) Gold nanoparticles: Assembly, supramolecular chemistry, quantum-size-related properties, and applications toward biology, catalysis, and nanotechnology. J Chem Rev 104:293–346
Das RK, Gogoi N, Bora U (2011) Green synthesis of gold nanoparticles using Nyctanthes arbor-tristis flower extract. Bioprocess Biosyst Eng 34:615–619
Das D, Nath BC, Phukon P, Dolui SK (2013) Synthesis and evaluation of antioxidant and antibacterial behavior of CuO nanoparticles. Colloids Surf B Biointerfaces 101:430–433
Das RK, Golder AK (2017) Co_3O_4 spinel nanoparticles decorated graphite electrode: Bio-mediated synthesis and electrochemical H_2O_2 sensing. Electrochimica Acta 251:415–426
Deparis O, Khuzayim N, Parker A, Vigneron JP (2009) Assessment of the antireflection property of moth wings by three-dimensional transfer-matrix optical simulations. Phys Rev E:79–87
Devi M, Devi S, Sharma V, Rana N, Bhatia RK, Bhatt AK (2019) Green synthesis of silver nanoparticles using methanolic fruit extract of Aegle marmelos and their antimicrobial potential against human. J Tradit Med Complement. https://doi.org/10.1016/j.jtcme.2019.04.007
Dubey SP, Lahtinen M, Sillanpaa M (2010) Tansy fruit mediated greener synthesis of silver and gold nanoparticles. Process Biochem 45(7):1065–1071
Duran N, Marcato PD, Alves OL, Souza GI, Esposito E (2005) Mechanistic aspects of biosynthesis of silver nanoparticles by several Fusarium oxysporum strains. J Nanobiotechnol 3:1–8
Dwivedi AD, Gopal K (2010) Biosynthesis of silver and gold nanoparticles using Chenopodium album leaf extract. Colloids Surf A 369(1–3):27–33
Edison JIETN, Sethuraman MG (2013) Electrocatalytic reduction of benzyl chloride by green synthesized silver nanoparticles using pod extract of Acacia nilotica. ACS Sustain Chem Eng 1:1326–1332
Elechiguerra JL, Reyes-Gasgab J, Yacaman MJ (2006) The role of twinning in shape evolution of anisotropic noble metal nanostructures. J Mater Chem 16:3906–3919
Elliott DW, Zhang W (2001) Field assessment of Nanoscale bimetallic particles for groundwater treatment. Environ Sci Technol 35:4922
Erjaee H, Rajaian H, Nazifi S (2017) Synthesis and characterization of novel silver nanoparticles using Chamaemelum nobile extract for antibacterial application. Adv Nat Sci Nanosci Nanotechnol 8:025004
Eustis S, Hsu HY, El-Sayed MA (2005) Gold nanoparticle formation from photochemical reduction of Au^{3+} by continuous excitation in colloidal solutions: A proposed molecular mechanism. J Phys Chem B 109(11):4811–4815
Fierascu I, Georgiev MI, Ortan A, Fierascu RC, Avramescu SM, Ionescu D, Sutan A, Brinzan A, Ditu LM (2017) Phyto-mediated metallic nano-architectures via Melissa officinalis L.: synthesis, characterization and biological properties. Sci Rep. https://doi.org/10.1038/s41598-017-12804-7
Fuhrer MS, Nygård J, Shih L, Forero M, Yoon YG, Mazzoni MSC, Choi HJ, Ihm J, Louie SG, Zettl A, McEuen PL (2000) Crossed nanotube junctions. Science 288:494
Gardea-Torresdey JL, Tiemann KJ, Gamez G, Dokken K, Tehuacamanero S, Jose-Yacaman M (1999) Gold nanoparticles obtained by bio-precipitation from gold (III) solutions. J Nanopart Res 1(3):397–404
Gericke M, Pinches A (2006) Biological synthesis of metal nanoparticles. Hydrometallurgy 83(1-4):132–140

Gopidas KR, Whitesell JK, Fox MA (2003) Synthesis, characterization and catalytic activity of a palladium nanoparticle cored dendrimier. Nano Lett 3:1757–1760
Heinlaan M, Ivask A, Blinova I, Dubourguier HC, Kakru A (2008) Toxicity of nanosized and bulk ZnO, CuO and TiO_2 to bacteria Vibrio fischeri and crustaceans Daphnia magna and Thamnocephalus platyurus. Chemosphere 71:1308–1316
Hrapovic S, Liu Y, Male KB, Luong JHT (2004) Electrochemical biosensing plate form using platinum nanoparticles and carbon nanotubes. Anal Chem 76:1083–1088
Huang J, Li Q, Sun D, Lu Y, Su Y, Yang X, Wang H, Wang Y, Shao W, He N (2007) Biosynthesis of silver and gold nanoparticles by novel sundried Cinnamomumcamphora leaf. Nanotechnol 18(10):105104:1–11
Hu XL, Wui S (2012) Synthesis of gold nanoparticles by solution plasma sputtering in various solvents. J Phys Conf Ser 417:012–030
Hwa KY, Subramani B (2014) Synthesis of zinc oxide nanoparticles on graphene-carbon nanotube hybrid for glucose biosensor applications. Biosens Bioelectron 62:127–133
Jiang RB, Li BX, Fang CH, Wang JF (2014) Metal/semiconductor hybrid nanostructures for plasmon-enhanced applications. Adv Mater 26:5274–5309
Kaviya S, Santhanalakshmi J, Viswanathan B, Muthumary J, Srinivasan K (2011) Biosynthesis of silver nanoparticles using citrus sinensis peel extract and its antibacterial activity. Spectrochim Acta A 79(3):594–598
Khan AA, Fox EK, Gorzny ML, Nikulina E, Brougham DF, Wege C, Bittner AM (2013) pH control of the electrostatic binding of gold and iron oxide nanoparticles to tobacco mosaic virus. Langmuir 29(7):2094–2098
Kuehner DE, Heyer C, Ramsch C, Fornefeld UM, Blanch HW, Prausnitz JM (1997) Interactions of lysozyme in concentrated electrolyte solutions from dynamic light-scattering measurements. Biophys J 73:3211–3224
Kulkarni N, Muddapur U (2014) Biosynthesis of metal nanoparticles: A review. J Nanotechnol 2014:1–8
Kumar A, Mandal S, Selvakannan PR, Parischa R, Mandale AB, Sastry M (2003) Investigation into the interaction between surface-bound alkylamines and gold nanoparticles. Langmuir 19:6277–6282
Lee HJ, Lee G, Jang NR, Yun JH, Song JY, Kim BS (2011) Biological synthesis of copper nanoparticles using plants extract. Nanotechnology 1:371–374
Lengke M, Ravel B, Fleet ME, Wanger G, Gordon RA, Southam G (2006) Mechanisms of gold bioaccumulation by filamentous cyanobacteria from gold (III) chloride complex. Environ Sci Technol 40(20):6304–6309
Li WR, Xie XB, Shi QS, Zeng HY, Yang O, Chen YB (2009) Antibacterial activity and mechanism of silver nanoparticles on Escherichia coli. Appl Microbiol Biotechnol 85:1115–1122
Li X, Xu H, Chen ZS, Chen G (2011) Biosynthesis of nanoparticles by microorganisms and their applications. J Nanomater 2011:1–16
Li Y, Zhang W, Niu J, Chen Y (2012) Mechanism of photogenerated reactive oxygen species and correlation with the antibacterial properties of engineered metal-oxide nanoparticles. ACS Nano 6:5164–5173
Liu Y, Choi H, Dionysiou D, Lowry GV (2005) Trichloroethene hydrodechlorination in water by highly disordered monometallic nanoiron. Chem Mater 17:5315
Lv Q, Zhang B, Xing X, Zhao Y, Cai R, Wang W, Gu Q (2017) Biosynthesis of copper nanoparticles using Shewanella loihica PV-4 with antibacterial activity: novel approach and mechanisms investigation. J Hazard Mater 347:141–149
Mafune F, Kohno J, Takeda Y, Kondow TJ (2001) Dissociation and aggregation of gold nanoparticles under laser irradiation. J Phys Chem B 105(38):9050–9056
Makarov VV, Love AJ, Sinitsyna OV, Makarova SS, Yaminsky IV, Taliansky ME, Kalinina NO (2014) Green nanotechnologies: Synthesis of metal nanoparticles using plants. Acta Naturae 6(1):35–44

Malik P, Shankar R, Malik V, Sharma N, Mukherjee TK (2014) Green chemistry based benign routes for nanoparticle synthesis. J Nanopart 2014:1–14

Malika M, Rao CV, Das RK, Giri AS, Golder AK (2016) Evaluation of bimetal doped TiO_2 in dye fragmentation and its comparison to mono-metal doped and bare catalyst. Appl Surf Sci 368:316–324

Mandal D, Bolander ME, Mukhopadhyay D, Sarkar G, Mukherjee P (2006) The use of micro-organisms for the formation of metal nanoparticles and their application. Appl Microbiol Biotechnol 69(5):485–492

Mehrotra N, Tripathi RM, Zafar F, Singh MP (2017) Catalytic degradation of dichlorvos using biosynthesized zero valent iron nanoparticles. IEEE Transac Nano Biosci 16(4):280–286

Melissa A, Jones M, Gunsolus IL, Murphy CJ, Haynes CL (2013) Toxicity of engineered nanoparticles in the environment. Anal Chem 85:3036–3049

Mittal AK, Chisti Y, Banerjee UC (2013) Synthesis of metallic nanoparticles using plants. Biotechnol Adv 31:346–356

Mitra S, Chandra S, Laha D, Patra P, Debnath N, Pramanik A, Pramanik P, Goswami A (2012) Unique chemical grafting of carbon nanoparticle on fabricated ZnO nanorod: antibacterial and bioimaging property. Mater Res Bull 47:586–594

Mukherjee P, Ahmad A, Mandal D, Senapati S, Sainkar SR, Khan MI, Ramani R, Parischa R, Ajayakumar PV, Alam M (2001) Bioreduction of AuCl4 ions by the fungus, Verticillium sp. and surface trapping of the gold nanoparticles formed. Angew Chem Int Ed 40(19):3585–3588.

Narayanan KB, Sakthivel N (2008) Coriander leaf mediated biosynthesis of gold nanoparticles. Mater Lett 62:4588–4590

Naveen AN, Selladurai S (2015) Tailoring structural, optical and magnetic properties of spinel type cobalt oxide (Co_3O_4) by manganese doping. Physica B 457:251–262

Nigussie GY, Tesfamariam GM, Tegegne BM, Weldemichel YA, Gebreab TW, Gebrehiwot DG, Gebremichel GE (2018) Antibacterial activity of Ag-doped TiO_2 and Ag-doped ZnO nanoparticles. Int J Photoenergy. https://doi.org/10.1155/2018/5927485

Njagi EC, Huang H, Stafford L, Genuino H, Galindo HM, Collins JB (2011) Biosynthesis of iron and silver nanoparticles at room temperature using aqueous sorghum bran extracts. Langmuir 27:64–271

Nutt MO, Hughes JB, Wong MS (2005) Designing Pd-on-au bimetallic nanoparticle catalysts for Trichloroethene Hydrodechlorination. Environ Sci Technol 39:1346

Oluwafemi OS, Revaprasadu N, Adeyemi OO (2010) A facile green synthesis of ascorbic acid-capped ZnSe nanoparticles. Coll Surf B Biointer 79:126–130

Padil VVT, Cerník M (2013) Green synthesis of copper oxide nanoparticles using gum karaya as a biotemplate and their antibacterial application. Int J Nanomedicine 8:889–898

Perez J, Bax L, Escolano C (2005) Roadmap report on nanoparticles. Willems & van den Wildenberg, Barcelona, Spain

Poinern GEJ, Le X, Chapman P, Fawcett D (2013) Green biosynthesis of gold nanometre scale plate using the leaf extracts from an indigenous Australian plant Eucalyptus macrocarpa. Gold Bull 46(3):165–173

Pollini M, Paladini F, Sannino A, Picca RA, Sportelli MC, Nicola C, Nitti MA, Valentini M, Valentini A (2008) Individual, social, and environmental influences associated with HIV infection among injection drug users in Tijuana, Mexico. J Acquir Immune Defic Syndr 47(3):369–76

Prathna TC, Chandrasekaran N, Raichur AM, Mukherjee A (2011) Kinetic evolution studies of silver nanoparticles in a bio-based green synthesis process. Colloids Surf A 377(1–3):212–216

Puvanakrishnan P, Park J, Chatterjee D, Krishnan S, Tunnel JW (2012) In vivo tumor targeting of gold nanoparticles: Effect of particle type and dosing strategy. Int J Nanomed 7:1251–1258.

Rao CV (2018) Bio-inspired route of metal nanoparticles synthesis and photocatalysts doping. Ph.D. Dissertation. IIT Guwahati, Guwahati

Rao CV, Golder AK (2016) pH dependent size control, formation mechanism and antimicrobial functionality of bio-inspired AgNPs. RSC Adv 6(98):95483–95493

Rao CV, Golder AK (2016) pH dependent size control, formation mechanism and antimicrobial functionality of bio-inspired AgNPs. RSC Adv 6:95483–95493

Rao CV, Golder AK (2019) One pot green synthesis of Pt, Co and Pt@Co core-shell nanoparticles using Sechium edule. J Chem TechnolBiotechnol 94:911–918

Rao CV, Bag SS, Golder AK (2017) A biosynthesis route to nearly spherical AgNPs using chayote fruit extract. Environ Prog Sustain Energy 36(1):192–199

Rao CV, Chakraborty S, Golder AK (2018) Ag-doping on TiO_2 using plant-based glycosidic compounds for high photonic efficiency degradative oxidation under visible light. J Mol Liq 271:380–388

Roopan SM, Bharathi A, Prabhakarn A, Rahuman AA, Velayutham K, Rajakumar G, Padmaja RD, Lekshmi M, Madhumitha G (2012) Efficient phytosynthesis and structural characterization of rutile TiO2 nanoparticles using Annona squamosa peel extract. Spectrochim Acta A Mol Biomol Spectrosc 98:86–90

Sadiq IM, Chandrasekaran N (2010) Mukherjee, studies on effect of TiO_2 nanoparticles on growth and membrane permeability of Escherichia coli, Pseudomonas aeruginosa, and Bacillus subtilis. A Curr Nanosci 6:381–387

Salomoni R, Léo P, Montemor A, Rinaldi B, Rodrigues M (2017) Antibacterial effect of silver nanoparticles in Pseudomonas aeruginosa. Nanotechnol Sci Appl 10:115

Santhoshkumar T, Rahuman A, Jayaseelan C, Rajakumar G, Marimuthu S, Kirthi AV, Velayutham K, Thomas J, Venkatesan J, Kim SK (2014) Green synthesis of titanium dioxide nanoparticles using Psidium guajava extract and its antibacterial and antioxidant properties. Asian Pac J Trop Med 7:968–976

Saravanakumar A, Peng MM, Ganesh M, Jayaprakash J, Mohankumar M, Jang HT (2017) Low-cost and eco-friendly green synthesis of silver nanoparticles using Prunus japonica (Rosaceae) leaf extract and their antibacterial, antioxidant properties. Artif Cells Nanomed Biotechnol 45:1165–1171

Sathishkumar M, Sneha K, Yun YS (2009) Palladium nanocrystals synthesis using Curcuma longa tuber extract. Int J Mater Sci 4:11–17

Saxena A, Tripathi R, Zafar F, Singh P (2012) Green synthesis of silver nanoparticles using aqueous solution of Ficus benghalensis leaf extract and characterization of their antibacterial activity. Mater Lett 67:91–94

Sharma JK, Srivastava P, Singh G, Akhtar MS, Ameen S (2015) Green synthesis of Co_3O_4 nanoparticles and their applications in thermal decomposition of ammonium perchlorate and dye-sensitized solar cells. Mater Sci Eng B 193:181–188

Smitha SL, Nissamudeen KM, Philip D, Gopchandran KG (2008) Studies on surface plasmon resonance and photoluminescence of silver nanoparticles. Spectrochim Acta Part A Mol Biomol Spectrosc 71:186–190

Song JY, Jang HK, Kim BS (2009) Biological synthesis of gold nanoparticles using Magnolia kobus and Diopyros kaki leaf extracts. Process Biochem 44(10):1133–1138

Sperling RA, Gil PR, Zhang F, Zanella M, Parak WJ (2008) Biological applications of gold nanoparticles. Chem Soc Rev 37:1896–1908

Starowiicz M, Stypula B, Banas J (2006) Electrochemical synthesis of silver nanoparticles. Electrochem Commun 8:227–230

Stephen JR, Macnaughton SJ (1999) Developments in terrestrial bacterial remediation of metals. Curr Opin Biotechnol 10(3):230–233

Subhankari I, Nayak PL (2013) Synthesis of copper nanoparticles using Syzygium aromaticum (cloves) aqueous extract by using green chemistry. World J Nano Sci Technol 2:14–17

Sun Q, Cai X, Li J, Zheng M, Chen Z, Yu CP (2014) Green synthesis of silver nanoparticles using tea polyphenols and their catalytic activity in degradation of acid red B. Colloids Surfaces A Physicochem Eng Asp 444:226–231

Sun H, He Q, She P, Zeng S, Xu K, Li J, Liang S, Liu Z (2017) One-pot synthesis of Au/TiO_2 yolk-shell nanoparticles with enhanced photocatalytic activity under visible light. J Colloid Interf Sci 505:884–891

Surendra T, Roopan SM, Arasu MV, Al-Dhabi NA, Rayalu GM (2016) RSM optimized Moringa oleifera peel extract for green synthesis of M. oleifera capped palladium nanoparticles with antibacterial and hemolytic property. J Photochem Photobiol B Biol 162:550–557

Sykora D, Kasicka V, Miksik I, Rezanka P, Zaruba K, Matejka P, Kral V (2010) Applications of gold nanoparticles in separation sciences. J Sep Sci 33(3):372–387

Tahir K, Nazir S, Li B, Khan AU, Khan ZUH, Ahmad A, Khan QU (2015) Biodirected synthesis of palladium nanoparticles using Phoenix dactylifera leaves extract and their size dependent biomedical and catalytic applications. J Photochem Photobiol B Biol 153:261–266

Torres-Chavolla E, Ranasinghe RJ, Alocilja EC (2010) Characterization and functionalization of biogenic gold nanoparticles for biosensing enhancement. IEEE Trans Nanobiotechnol 9(5):533–538

Treguer M, Cointet C, Remita H, Khatouri J, Mostafavi M, Amblard J, Belloni JJ (1998) Dose rate effect on radiolytic synthesis of gold-silver bimetallic clusters in solution. J Phys Chem B 102(22):4310–4321

Tripathi RM, Chunga SJ (2019) Biogenic nanomaterials: synthesis, characterization, growth mechanism and biomedical applications. J Microbiol Methods 157:65–80

Tripathi R, Bhadwal AS, Gupta RK, Singh P, Shrivastav A, Shrivastav B (2014) ZnO nanoflowers: novel biogenic synthesis and enhanced photocatalytic activity. J Photochem Photobiol B Biol 141:288–295

Tripathi DK, Shivesh PA, Kumar SD, Nawal C, Dubey K (2018) Nanomaterials in Plants, Algae and Microorganisms: Concepts and Controversies 1:382–386

Tu WG, Zhou Y, Li HJ, Li P, Zou ZG (2015) Au/TiO_2 yolk-shell hollow spheres for plasmon-induced photocatalytic reduction of CO_2 to solar fuel via a local electromagnetic field. Nanoscale 7:14232–14236

Vijayakumar S, Krishnakumar P, Arulmozhi P, Mahadevan S, Parameaswari N (2018) Biosynthesis, characterization and antimicrobial activities of zinc oxide nanoparticles from leaf extract of Glycosmis pentaphylla (Retz.) DC. Microb Pathog 116:44–48

Wang CB, Zhang W (1997) Synthesizing Nanoscale Iron particles for rapid and complete dechlorination of TCE and PCBs. Environ Sci Technol 31:2154

Wang L, Chen X, Zhan J, Chai Y, Yang C, Xu L, Zhuang W, Jing B (2005) Synthesis of gold nano and microplates in hexagonal liquid crystals. J Phys Chem B 109:3189–3194

Wechtersbach L, Cigic B (2007) Reduction of dehydroascorbic acid at low pH. J. Biochem Biophys Methods 70:767–772

Yilmaz M, Turkdemir H, Kilic MA, Bayram E, Cicek A, Mete A, Ulug B (2011) Biosynthesis of silver nanoparticles using leaves of Stevia rebaudiana. Mater Chem Phys 130:1195–1202

Yude W, Shuo Z, Xinghui W, Qingju L (2006) Synthesis and optical properties of nano-ZnO particles/mesostructured SnO_2 composite. Mater Chem Phys 98:121–124

Zhang G, Wang DJ (2008) Fabrication of heterogeneous binary arrays of nanoparticles via colloidal lithography. J Am Chem Soc 130(17):5616–5617

Zhang F, Wu X, Chen Y, Lin H (2009) Application of silver nanoparticles to cotton fabric as an antibacterial textile finish. Fibers and Polymers 10(4):496–501

Zhang N, Liu SQ, Xu YJ (2012) Recent progress on metal core at semiconductor shell nanocomposites as a promising type of photocatalyst. Nanoscale 04:2227–2238

Zhang A, Liu M, Liu M, Xiao Y, Li Z, Chen J, Sun Y, Zhao J, Fang S, Jia D, Li JF (2014) Homogeneous Pd nanoparticles produced in direct reactions: green synthesis, formation mechanism and catalysis properties. Mater Chem A 2:1369–1374

Zhong J, Chen F, Zhang JL (2010) Carbon-deposited TiO_2: synthesis, characterization, and visible photocatalytic performance. J Phys Chem C 114:933–939

Zhou H, Ding L, Fan TX, Ding J, Zhang D, Guo QX (2014) Leaf-inspired hierarchical porous CdS/Au/N-TiO_2 heterostructures for visible light photocatalytic hydrogen evolution. Appl Catal B Environ 147:221–228

Zuas O, Hamim N, Sampora Y (2014) Bio-synthesis of silver nanoparticles using water extract of Myrmecodia pendan (Sarang Semut plant). Mater Lett 123:156–159